Interaction Simulation of a Lateral Wall Distance on Aerodynamic Characteristics of a Simplified High-speed Train

Alireza Hajipour[1*], Arash Mirabdolah Lavasani[1], Mohammad Eftekhari Yazdi[1]

[1] Department of Mechanical Engineering, Central Tehran Branch, Islamic Azad University, 1469669191 Tehran, Iran
* Corresponding author, e-mail: alirezahajipour.eng@iauctb.ac.ir

Abstract

The natural features, such as mountain slopes, cliffs, and the human-made artificial walls, such as train station walls, windbreakers, and even residential and office buildings, can affect the movement structure of high-speed trains. In the present paper, using computational fluid dynamics (CFD), the interaction of lateral wall distances on the aerodynamic characteristics of a high-speed train is simulated. To achieve this -using OpenFOAM- the governing equations are solved. Also, the used solver is simpleFoam which the Simple algorithm (Semi-Implicit Method for Pressure Linked Equations) is applied to decouple the Navier-Stokes's equations. In the following a simplified high-speed train is considered, combining Reynolds-Averaged Navier-Stokes (RANS) equations and k-ω (SST) turbulence approach, an incompressible turbulent air-flow around it is simulated. Also, the flow and aerodynamic structures affected by distance changes between the lateral wall and the train are analyzed. Therefore, the lift, drag, and side aerodynamic forces and their corresponding moments as pitching, yawing, and rolling are provided and compared for four distance cases. In the following, the most significant components of flow structure, such as streamlines, velocity and pressure distributions, and vortices structures, are discussed. Finally, using the turbulent kinetic energy analysis, the air-flow's turbulent level around the train, especially in critical areas, is investigated. The findings illustrated that the closer distance between the train and the wall has more destructive effects on the movement of the high-speed trains. The results of the present study can be helpful for designing structures along the rail and distancing it from natural features.

Keywords

high-speed train, aerodynamics, turbulence, lateral wall, openFOAM

1 Introduction

In recent years, high-speed trains have made extensive progress, and so, the various issues and problems about them have been investigated and modified, consequently. One of the hundreds of issues facing high-speed trains that need to be explored and optimized is the existence of natural and artificial walls parallel to the route of high-speed trains. Since natural and artificial walls have direct and profound effects on the movement characteristics of vehicles, especially high-speed trains, it is crucial to investigate their characteristics in the movement of trains. The walls of train stations, natural features of the route, windbreakers, and even buildings near the railways are the most important examples of these walls. All the samples have profound and significant effects on the movement of high-speed trains, especially their aerodynamic characteristics. Hence, in the last decade, various studies have been

performed on high-speed trains [1], their aerodynamic characteristics, and especially their multiple obstacles, which some of the most important of which are as follows:

In 2010, a numerical simulation of two high-speed trains passing each other at a similar velocity by a new approach was provided by Zhao and Sun [2]. In this study, Fluent commercial software is employed to simulate pressure waves and flow fields. In the same year, Baker [3] provided a comprehensive investigation of the aerodynamic behavior of a high-speed train. Flow fields around the nose, side, roof, and under the train and wake of the train were simulated. Moreover, the surface pressure of the train for the variety of the train velocity was shown. Bell et al. [4], in 2014, using a wind tunnel, investigated the wake and slipstream of a high-speed train. In this study, the full details of the wake phenomenon and

characteristics of the slipstream due to the train velocity and turbulent air-flow around it are described. Also, the effects of rail configuration on wake are analyzed. In the same year, Shuanbao et al. [5], relying on train geometry, optimized the aerodynamic parameters of a high-speed train. To achieve this, a CRH380A high-speed train was considered, and a practical multi-objective optimization was done via a genetic algorithm (GA) and cross-validation methods. Eventually, the aerodynamic drag and side forces in the optimized geometry were less than the original one. Since the Reynolds number has a profound effect on the aerodynamic behavior of high-speed vehicles, Niu et al. [6], in 2016, investigated the effect of the Reynolds number on the aerodynamic performance and pressure of a high-speed train, experimentally. Along with this, the yaw angles' effects as 0 to 15 degrees for two scales of trains were investigated. Also, the Reynolds number changes on the lift force and pressure coefficient were analyzed in more detail. A comparison among three turbulence models, IDDES, RANS, and SAS, to an aerodynamic simulation of air-flow around a high-speed train was made by Munoz-Paniagua et al. [7] in 2017. Aerodynamic forces and pressure distribution of the train body, streamlines, and other flow key parameters considering crosswind for the three turbulence models were investigated and compared. Also, the best simulation model in the case was identified with the lowest computational cost. In 2017, Bell et al. [8] studied the effects of tail angle on the flow structure of a generic high-speed train. In this experimental research, a variation of the roof angle of the train tail on the wake-field and the related slipstream were analyzed. A numerical simulation of the influences of the nose geometry on the aerodynamic behavior of a high-speed train was performed by Niu et al. [9] in 2018. In this study, two train cases with two nose types, short and long length, were considered, and the effects of their changes on critical parameters of air-flow were analyzed. Flow structure, pressure, and velocity distributions, boundary layer and aerodynamic forces around the high-speed train, were illustrated, and a comparison with the obtained results of experimental data was performed. In the same year, Xia et al. [10] focused on the wake phenomenon and its related properties of a 1:50 scale high-speed train via an experimental setup. The flow and pressure results of the wind tunnel were done by particle image velocimetry (PIV) and Hot-wire anemometry. The results indicated the location and extent of the wake phenomenon. In 2018, the influences of moving high-speed trains in the open-air on wind formation and its effects on the people and structures were reported by Rocchi et al. [11]. A multi-objective optimization of aerodynamic design of high-speed railway windbreaks using LBM and wind tunnel test results was provided by Mohebbi and Rezvani [12, 13] in 2018. In these researches, LBM simulations are combined with the Multi Objective Genetic Algorithm for aerodynamic design and characteristics of a high-speed railway windbreak. Mohebbi and Rezvani [14] also in 2018 performed effects of air fence geometry on air-flow around an ICE3 high-speed train on a double-line railway track with exposure to crosswinds. This research is concerned with finding a proper solution for attenuating the worrying effects of the winds that hit the trains based on the Lattice-Boltzmann method. In the extensive investigation, some of the significant railway equipment, such as safety ones, were considered to investigate the effects of wind flow generated by the train. Li et al. [15], in 2019, using an experimental setup, investigated the aerodynamic properties of a streamlined deck of a high-speed train under crosswind. In this case, the yaw angles of air-flow and their effects on the aerodynamic characteristics of the train were simulated. Also, the flow pattern, shear stress, pressure distribution, and other flow key parameters were analyzed. An origami optimization on the design structure of a high-speed train was performed by Wang et al. [16] in 2019. They focused on the crashworthiness of a multi-cell thin-walled structure in the event of an accident. Hashmi et al. [17] in 2019 reported and analyzed the crosswind effects on windbreakers of high-speed trains. In this case, a 1:25 train model of Class 390 Pendolino was considered. Influences of yaw angle variation on the turbulent flow around it and then on the windbreakers in the wind tunnel were simulated. Finally, the most suitable conditions for wind yaw angles and the windbreakers' angles were specified. In 2020, an experimental-numerical investigation of a high-speed train was performed by Zampieri et al. [18]. Since, high-speed moving of trains creates strong inductive air-flow that can damage infrastructures and people close to it, one of the main objectives of this study was to study and reduce the air-flow damage caused by train movement. So, at first, an experimental setup was applied, and its data was reported and then, using CFD, a numerical simulation of turbulent air-flow around the high-speed train was done. For validation, a comparison with experimental results was performed. Dong et al. [19] in 2020, studied the influence of ground distance on the aerodynamic properties of

a simplified high-speed train. In this case, four distances from the ground to the train were considered, and flow structure, aerodynamic forces, and wake phenomenon due to turbulent air-flow between the train and the ground were simulated, and investigated. In 2020, a numerical analysis of the aerodynamic and dynamic effects of a huge vortex on a movement high-speed train was done by Xu et al. [20]. Using the DES numerical method, a tornado vortex and its effect on the high-speed train were simulated. In this study, in addition to the aerodynamic components of the flow, the dynamic parameters due to dynamic tornado loads also were analyzed. Muñoz-Paniagua and García [21] in 2020, did an optimization on the aerodynamic force of a high-speed train. To achieve this, an aerodynamic drag optimization on the nose geometry of the high-speed train was performed. For the optimization, a genetic algorithm method was applied, and the optimal values of the aerodynamic drag were reported and analyzed. The influences of the variation of Reynolds number on the wake phenomenon of a high-speed train were investigated by Wang et al. [22] in 2020. Then, the behaviors of the velocity, pressure, vortex structure, and streamlines of the considered high-speed train for different five Reynolds numbers were analyzed. The aerodynamic performance of a high-speed train under the platform influence was investigated by Xiao et al. [23] in 2020. In this study, the pantograph as one of the important components of a high-speed train was considered. The effect of some geometrical specifications on the lift and drag aerodynamic forces was presented. Also, the influence of it on the pressure distribution of the train surface was reported. An experimental investigation of aerodynamic pressure on a moving high-speed train was performed by Xiong et al. [24] in 2020. Using pressure sensors, the transient aerodynamic characteristics of the inner area were measured. In the same year, Li et al. [25] investigated the influences of the numerical divergence methods on the turbulent air-flow around high-speed trains. Since the divergence method has serious effects on the numerical simulation accuracy, four prevalent divergence approaches were used to predict the aerodynamic characteristics of a high-speed train against a crosswind. Linear-upwind stabilized transport, second-order limited-linear differencing, linear-upwind differencing, and first-order upwind differencing where the divergence methods were applied and analyzed in this study. Moreover, the numerical results were compared with the related experimental data. From 2021 to 2023,

Mohebbi and Safaee [26]; Mohebbi and Rezvani [27]; and Mohebbi et al. [28, 29] in a series of parallel researches, performed influences of fences on the aerodynamic behaviors of a high-speed train using the Lattice Boltzmann Method. In the following, the porous wind barriers that are widely used in this industry have been investigated and compared. Also, to decrease the harmful influences of crosswinds, the work attempted to find an optimum porous barrier design. Finally, Hajipour et al. [30–32] in 2021 investigated the impacts of some wall functions on the airflow and aerodynamic properties of a simplified high-speed train using OpenFOAM. They studied the implemented wall function, known as the Enhanced Wall Function, which would be helpful in high-speed train aerodynamic simulations.

As mentioned, in recent years, various researches have been conducted on the high-speed train and other features related to its movement, Still, the effect of lateral walls along the movement of the train was not sufficiently addressed. For this reason, this research has addressed this relatively neglected sector. And since, the destructive loads from lateral winds, both forces and moments, may cause the train to derail; the importance of lateral walls and their distances in the movement and safety of high-speed trains seems to be doubled. Thus, in the present study using Reynolds-Averaged Navier-Stokes (RANS), the effects of lateral walls and their distances on the aerodynamic characteristics of turbulent air-flow around a simplified high-speed train are simulated. Also, the results of the space changes on the flow and aerodynamic structure are discussed, and the destructive and resistant phenomena to the train movement are analyzed. At the end, the turbulent level, especially in the critical area, is specified.

As mentioned, using CFD, the interaction of lateral wall distances on the aerodynamic characteristics of a high-speed train is simulated. To achieve this, a simplified high-speed train is considered, and combining RANS equations and k-ω (SST) turbulence approach, an incompressible turbulent air-flow around it is simulated. With a cursory glance at the results, they illustrated that reducing the distance between them increases opposition forces and moments. Also, the principal parameters of flow structure, i.e., streamline, velocity and pressure distributions, and vortices structures, are shown. Finally, the contour of the turbulent kinetic energy as an essential parameter in detecting the degree of turbulence for the four cases is presented.

2 Numerical simulation overview

In this study, using the open-source OpenFOAM package [33], the governing equations are solved. Also, the used solver is simpleFoam, in which the Simple algorithm (Semi-Implicit Method for Pressure Linked Equations) is applied to decouple Navier-Stokes's equations [34].

Moreover, using the standard second-order central differencing and the second-order upwind schemes, the diffusion and convection terms are discretized, respectively [34].

The geometrical details of the simplified high-speed train and the computational domain are shown in Fig. 1. Since practical and real high-speed trains have complicated geometries, they are not used for aerodynamic analysis. Instead, the simplified high-speed train can be used in numerical and experimental research [35–39]. As can be seen, a simplified high-speed train model with length (*L*), width (*d*), and height (*d*) and the distance from the lateral wall (*S*) are specified. Moreover, in this case, based on the velocity (70 m/s) and the train geometry (*d* = 0.56 m), the Reynolds number of turbulent air-flow around the train is specified as Re = 2.6×10^6 and the kinematic viscosity is $v = 1.5 \times 10^{-5}$ m²/s.

In the present study, the effect of the lateral wall distance on aerodynamic characteristics of a simplified high-speed train is investigated. To achieve this, four practical distance ratios of *S*/*d* = 0.25, 0.5, 0.75, and 1 (in which *S* and *d* are the train distance from the lateral wall and the width of the cross-section of the train, respectively) in Fig. 1. are considered and aerodynamic simulation on them is analyzed.
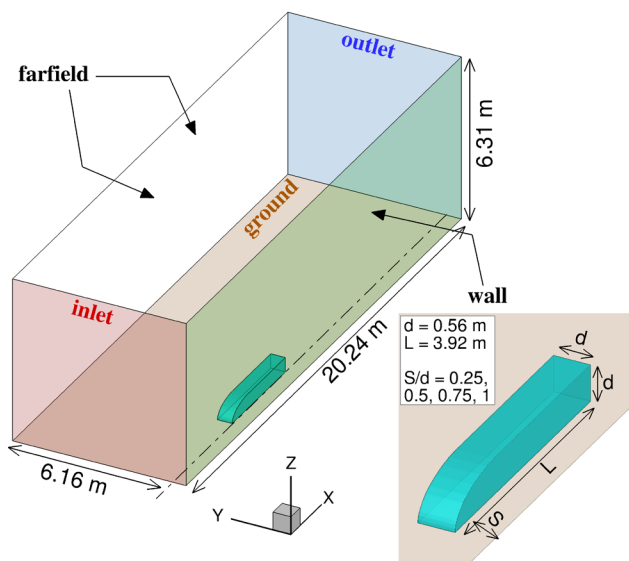
Also, the boundary conditions of the problem are defined as follows: constant velocity for the inlet, ground, and wall is considered. For the walls of the high-speed train, the no-slip condition is assumed. Slip boundary condition is applied on the far field boundaries, and zero gradient is used at the outlet. Moreover, the outlet pressure value is adopted zero, and for the other boundaries, zero gradient is considered. Further details of the boundary conditions are shown in Fig. 1. Besides, the turbulent intensity is defined as about 1% for the inlet, and for the walls, *omegaWallFunction* and *kqRWallFunction*, which are standard wall functions of OpenFOAM, are used. In the case without the lateral wall, due to the symmetry of the geometry, the symmetric boundary condition is used on the middle plane to reduce the computational cost.

The cells in the numerical simulation are generated via a structured, uniform Cartesian mesh by blockMesh, an essential meshing tool in OpenFOAM. Further mesh refinement is applied close to the train body, and around areas using the mesh generation utility of the *SnappyHexMesh* tool, which is also supplied with OpenFOAM. In the present study, the simulation is done with almost 2 million cells in each case for the computational domain, as shown in Fig. 2. Also, In the case without the lateral wall, the number of cells is decreased to 1.2 million due to the symmetry plane. Finally, Fig. 3 illustrates the residual error for different parameters of the paper. According to Fig. 3, all values and parameters used in the numerical calculation are converged.

3 Equations

3.1 Governing equations

In this manuscript, an incompressible, three-dimensional, and turbulent air-flow around a simplified high-speed train is considered. Then, combining Reynolds-Averaged Navier-Stokes (RANS) equations with the *k-ω* (SST) turbulence methods, the air-flow around the train is simulated.
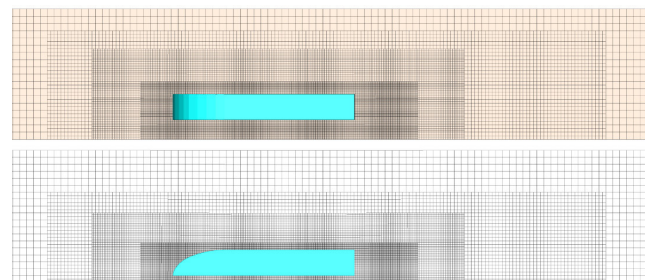

Fig. 1 Geometrical details of the simplified high-speed train and the computational domain

Fig. 2 Top and side views of the mesh structure in the computational domain
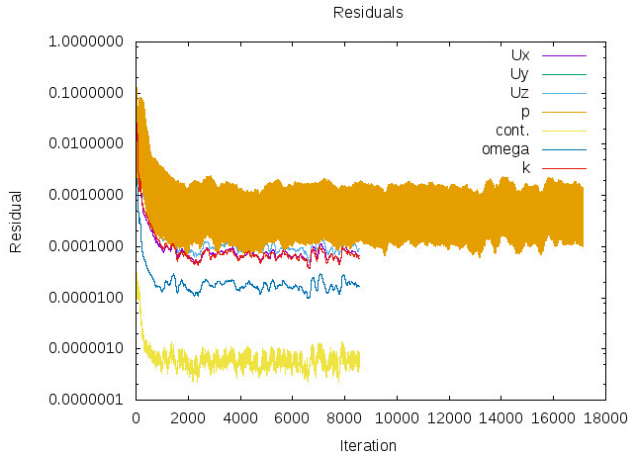
Fig. 3 Residual error for different parameters

Based on the solution approach, the continuity and momentum equations can be written by Eq. (1) and Eq. (2) [34]:

$$\frac{\partial u_j}{\partial x_j} = 0 \tag{1}$$

$$\frac{\partial u_i}{\partial t} + \frac{\partial u_i u_j}{\partial x_j} = -\frac{1}{\rho}\frac{\partial P}{\partial x_i} + \frac{\partial \tau_{ij}}{\partial x_j}. \tag{2}$$

Where, ρ, P, and u_i are the density, pressure, and the velocity in ith direction. Also, the effective stress tensor, τ_{ij}, can be defined by Eq. (3) [34]:

$$\tau_{ij} = \left(v + v_t\right)\left[\frac{\partial u_i}{\partial x_j} + \frac{\partial u_j}{\partial x_i} - \frac{2}{3}\frac{\partial u_k}{\partial x_k}\delta_{ij}\right]. \tag{3}$$

Where, v, v_t, and δ are the kinematic viscosity, turbulent kinematic viscosity, and the Kronecker Delta, respectively [34]. Also, the specific dissipation rate (ω) is in Eq. (4):

$$\frac{\partial \omega}{\partial t} + U_j\frac{\partial \omega}{\partial x_j} = \alpha S^2 - \beta \omega^2 + \frac{\partial}{\partial x_j}\left[\left(v + \sigma_\omega v_T\right)\frac{\partial \omega}{\partial x_j}\right]$$
$$+ 2\left(1 - F_1\right)\sigma_{\omega 2}\frac{1}{\omega}\frac{\partial k}{\partial x_i}\frac{\partial \omega}{\partial x_i}. \tag{4}$$

Where, v_t is calculated by the k-ω (SST) turbulence model in this study [34].

$$v_t = \frac{\alpha_1 k}{\max\left(\alpha_1 \omega, SF_2\right)} \tag{5}$$

The following closure coefficient is applied in the research:

$$F_2 = \tanh\left[\left[\max\left(\frac{2\sqrt{k}}{\beta^* \omega y}, \frac{500v}{y^2 \omega}\right)\right]^2\right]. \tag{6}$$

Where, y is the space to the next surface. Also, the other closure coefficients and auxiliary relations are as follows:

$$P_k = \min\left(\tau_{ij}\frac{\partial U_i}{\partial x_j}, 10\beta^* k\omega\right) \tag{7}$$

$$F_1 = \tanh\left\{\left\{\min\left[\max\left(\frac{\sqrt{k}}{\beta^* \omega y}, \frac{500v}{y^2 \omega}\right), \frac{4\sigma_{\omega 2} k}{CD_{k\omega} y^2}\right]\right\}^4\right\} \tag{8}$$

$$CD_{k\omega} = \max\left(2\rho\sigma_{\omega 2}\frac{1}{\omega}\frac{\partial k}{\partial x_i}\frac{\partial \omega}{\partial x_i}, 10^{-10}\right) \tag{9}$$

$$\phi = \phi_1 F_1 + \phi_2\left(1 - F_1\right) \tag{10}$$

$$\alpha_1 = \frac{5}{9}, \quad \alpha_2 = 0.44 \tag{11}$$

$$\beta_1 = \frac{3}{40}, \quad \beta_2 = 0.0828, \quad \beta^* = \frac{9}{100} \tag{12}$$

$$\sigma_{k1} = 0.85, \quad \sigma_{k2} = 1, \quad \sigma_{\omega 1} = 0.5, \quad \sigma_{\omega 1} = 0.856. \tag{13}$$

3.2 Aerodynamic equations

A high-speed train experiences different aerodynamic forces and coefficients while passing through a turbulent air-flow that includes the lift (F_L), drag (F_D), and side (F_S) forces [35]. The lift force is a force that intends to raise the train of the ground, the drag force is an opposite force of the train moving forward, and the side force is a force on the side of the train. Based on the disruptions, the lift, drag, and side forces as coefficients are defined by Eqs. (14)–(16) [37]:

$$C_L = \frac{F_L}{\frac{1}{2}\rho U_\infty^2 A} \tag{14}$$

$$C_D = \frac{F_D}{\frac{1}{2}\rho U_\infty^2 A} \tag{15}$$

$$C_S = \frac{F_S}{\frac{1}{2}\rho U_\infty^2 A} \tag{16}$$

Where, U_∞ and ρ are the free-stream velocity and density of the air-flow, F_L, F_D, and F_S are the lift, drag, and side forces, C_L, C_D, and C_S are the lift, drag, and side coefficients, A is the surface of the train.

Moreover, there are aerodynamic moments corresponding with the aerodynamic forces as pitching (R_{PT}), yawing (R_Y), and rolling (R_{RL}) moments, respectively, which are shown in Fig. 4 described by Eqs. (17)–(19) [37]:
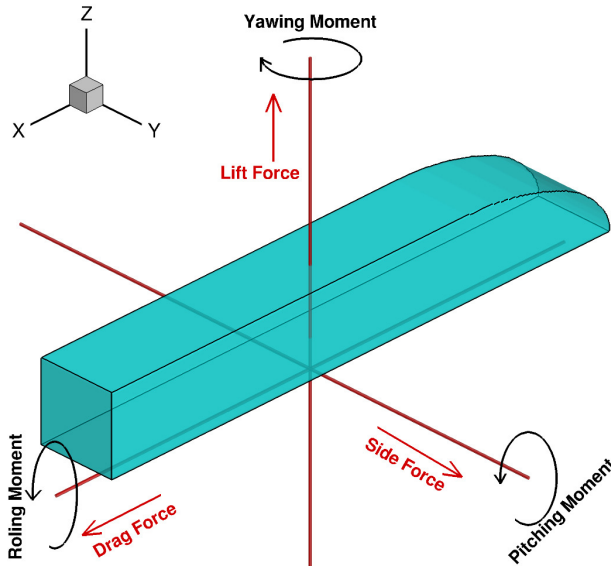
Fig. 4 Details of aerodynamic forces (lift, drag, and side) and their corresponding moments (pitching, yawing, and rolling)

Fig. 5 Grid independence for the four grids (Grid 1: coarse, Grid 2: medium, Grid 3: fine, and Grid 4: fine) using aerodynamic drag and lift coefficients

$$C_{PT} = \frac{R_{PT}}{\frac{1}{2}\rho U_\infty^2 AL} \qquad (17)$$

$$C_Y = \frac{R_Y}{\frac{1}{2}\rho U_\infty^2 AL} \qquad (18)$$

$$C_{RL} = \frac{R_{RL}}{\frac{1}{2}\rho U_\infty^2 AL}. \qquad (19)$$

Where, R_{PT}, R_Y, and R_{RL} are the pitching, yawing, and rolling moments, C_{PT}, C_Y, and C_{RL} are the pitching, yawing, and rolling moment coefficients, respectively. Moreover, L is the height of the train.

4 Grid independency

The numerical model's programming and computational activity are validated using grid sensitivity analysis. Meshes should be used that are independent. In the present study, to demonstrate mesh independence, two aerodynamic parameters, drag C_D, and lift C_L, coefficients, are considered, and this analysis has been done for them. As shown in Fig. 5, the drag coefficient is not sensitive to the grid-scale but the lift coefficient is exposed to the grid. So, to gain mesh independence, we considered it smaller than the previous one. As illustrated in Fig. 5, in the most minor grids (Grids 3 and 4), the obtained values for the drag and lift coefficients were independent of the number of cells and to reduce the computational costs, the third grid is used. It is worth mentioning the total number of cells for
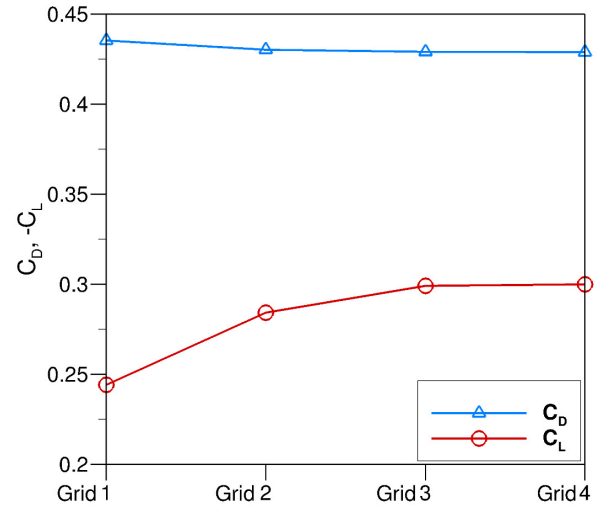
Grid 1, Grid 2, Grid 3, and Grid 4 are 150,000, 600,000, 1,000,000, and 1,300,000, respectively. Generally, according to the independence and computational costs, the third grid (Grid 3) is the most optimal and is used.

5 Results and discussion
5.1 Validation
For validation, some of the previous research is considered, and the characteristics of air-flow, geometry, and their computational domain are detailed in the Appendix. A comparison among the aerodynamic drag coefficients for validation is provided in Table 1 [40–44].

In the present study, the lateral wall effect on a three-dimensional turbulent air-flow around a simplified high-speed train is carried out. To find out more details of the case; first, the results of some of the most critical aerodynamic forces such as lift, drag, and side, and, their corresponding moments are examined, and then, the most significant flow characteristics such as streamlines, velocity and pressure distributions and turbulent kinetic energy are discussed.

Table 1 Validation comparison among the aerodynamic drag coefficients for the previous studies and results of this paper

Cases	Aerodynamic Drag Coefficient (C_D)
Wang et al. [40]	1.189
Nakaguchi [41]	1.170
Raul and Bernard [42]	1.170
Anderson [43]	1.090
Haider and Levenspiel [44]	1.040
Present paper	1.115

5.2 Aerodynamic forces

Due to the equation section of this study (Section 3.2 Aerodynamic equations), Fig. 6 compares the aerodynamic lift, drag, and side forces for the four defined distances on the lateral walls of the train as $S/d = 0.25$, 0.5, 0.75, and 1. As can be seen, the values of drag and lift aerodynamic coefficients for the different distances of the train to the lateral wall are almost constant and have imperceptible changes. The distance changes between the train body and the lateral wall have the most negligible effect on the drag and lift aerodynamic coefficients. But, for the side aerodynamic coefficient, as expected, when the distance between the train and the lateral wall increases, the effect of lateral loads increases, and consequently, the aerodynamic side coefficient increases. So, the maximum and minimum values of the side coefficients occur on $S/d = 0.25$, and $S/d = 1$, respectively. Fig. 6 illustrates the aerodynamic side force has tripled from the lowest (the minimum distance between the train and the lateral wall) to the highest (the maximum distance between the train and the wall) values.

In the following, Figs. 7, 8, and 9 show the influences of the distances between the train and the lateral wall on the pitching, yawing, and rolling aerodynamic moments, respectively. Fig. 7 shows that the pitching moment changes versus the distance's oscillations between the train and the lateral wall. The pitching moment values first, it has an ascending slope and after reaching the maximum point i.e., $S/d = 0.5$, continues a descending path to the end, i.e., $S/d = 1$. As mentioned, the maximum and the minimum values of the pitching moment occur on $S/d = 0.5$,
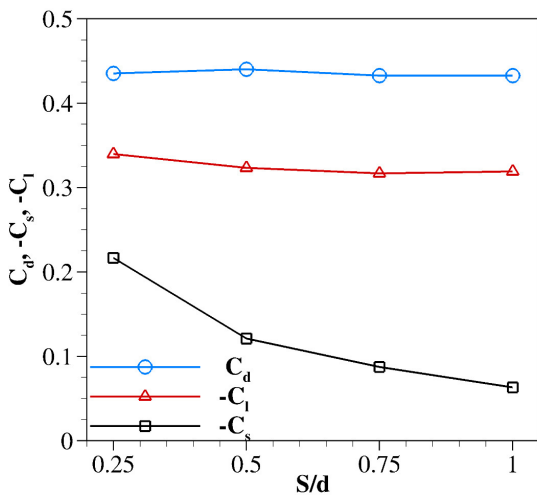

Fig. 7 Comparison of pitching moment (R_{PT}) for the four defined distances of the lateral walls of the train

Fig. 8 Comparison of yawing moment (R_Y) for the four defined distances of the lateral walls of the train

Fig. 6 Comparison among the lift (C_L), drag (C_D), and side (C_S) aerodynamic coefficients for the four defined distances of the lateral walls of the train
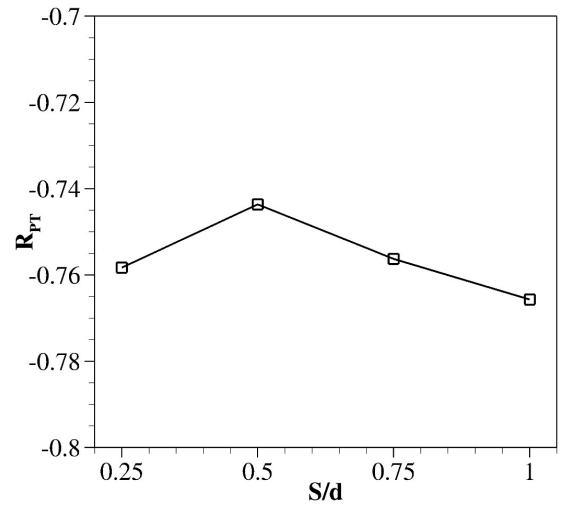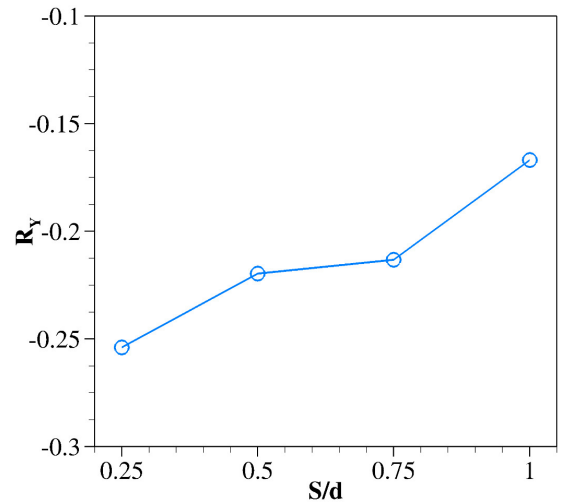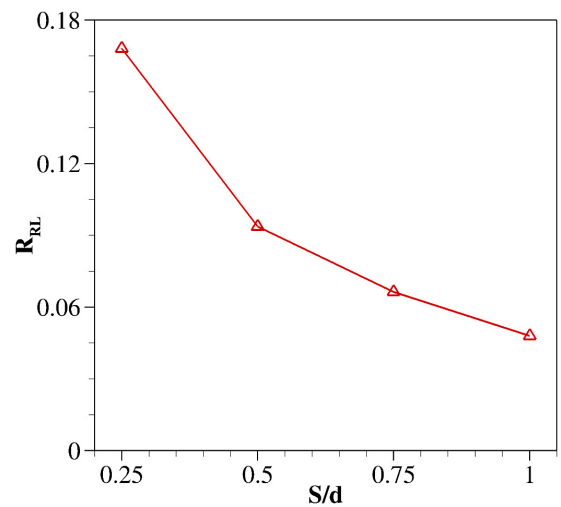

Fig. 9 Comparison of rolling moment (R_{RL}) for the four defined distances of the lateral walls of the train

and $S/d = 1$, respectively. The yawing moment changes are shown in Fig. 8. As the distance increases, this parameter increases, too. Also, the rolling moment changes are illustrated in Fig. 9. Its changes have an inverse ratio with increasing the distance. The rolling moment with decreasing the distance between the train and the wall increases it triples. Although all three moments are influential, on the train movement, the rolling moment is very effective in derailing the train.

5.3 Flow characteristics

Identification of fluid flow behavior is provided by various parameters. In the present study, some of the crucial and fundamental characteristics of the turbulent air-flow around the high-speed train are examined considering the lateral wall. Fig. 10 shows the two-dimensional streamlines around the high-speed train for the four distances between the train and the lateral wall in the side view as $S/d = 0.25$, 0.5, 0.75, and 1. Observing the comparison among the cases, as the distance between the lateral wall and the train increases, the size and intensity of the produced vortices behind the train increase, too. Also, as the distance increases (the meaning of increase is increase in this range), the possibility of vortex formation in the air distance between the train and the ground has increased, and larger flow separations are created. So, there is a giant vortex and a fundamental flow separation in the case of $S/d = 1$. It is predicted that the size and quality of the production vortex will go through a curve with extremes, which will be smaller ($S/d = 0.25$) and

then larger ($S/d = 1$) and decrease again until it reaches zero for distances far from the target range. In the following, Fig. 11 illustrates the two-dimensional streamlines around the high-speed train for the four distances between the train and the lateral wall in the top view as $S/d = 0.25$, 0.5, 0.75, and 1. The results show that if the distance between the train and the lateral wall increases, the air-flow is more symmetrical on the nose of the train, and in the same way, for the shorter distance between them, the air-flow structure is slightly closer to the wall. Also, when the wall is closer to the train, the produced vortices at the train's back become more elongated.

Figs. 12 and 13 show the velocity fields of the turbulent air-flow around the train for the four distances between the train and the wall. In Figs. 12 and 13, the velocity components in the x and y directions for the mentioned situation are provided. Fig. 12 illustrates the velocity field in the x-direction, U_x, for the four cases. It is quite clear that changes in the distances between the train and the lateral wall have significant effects on the velocity in the x-direction. Considerable areas are affected between the train and the back of the train. Similarly, Fig. 13 shows the velocity field in the y-direction, U_y. Similarly, the influences of the distances on the velocity structure, especially the areas between the train and the lateral wall, are significant. In fact, with decreasing the distance between the train and the wall, the vortices resulting from the velocity effect around the train increase, and then there is a possibility of more destructive impact on the train body.
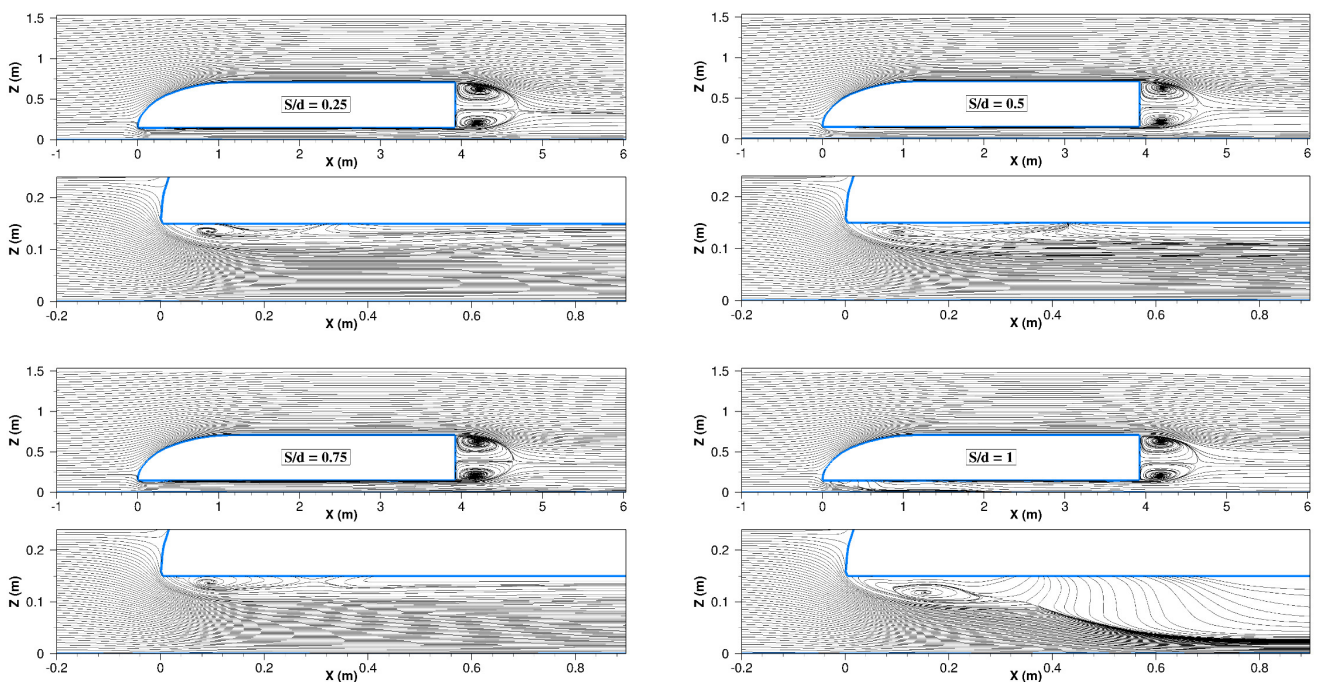

Fig. 10 Two-dimensional streamlines for the four distances between the train and the lateral wall in the side view
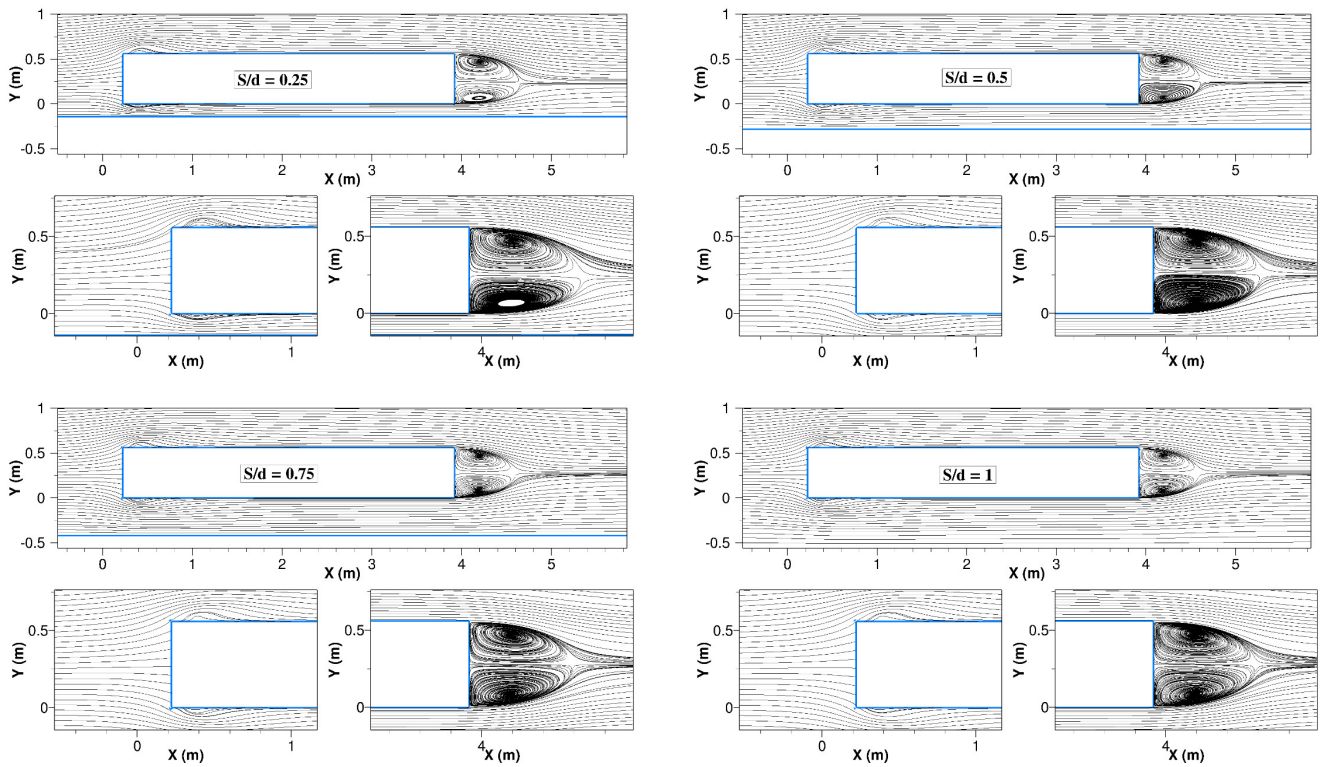
Fig. 11 Two-dimensional streamlines for the four distances between the train and the lateral wall in the top view
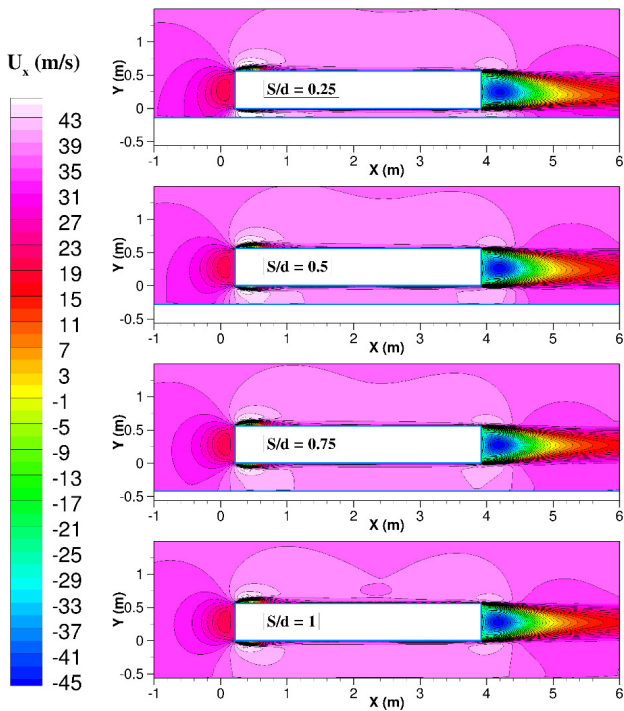

Fig. 12 Velocity field in the x-direction, U_x, for the four distances between the train and the lateral wall in the top view
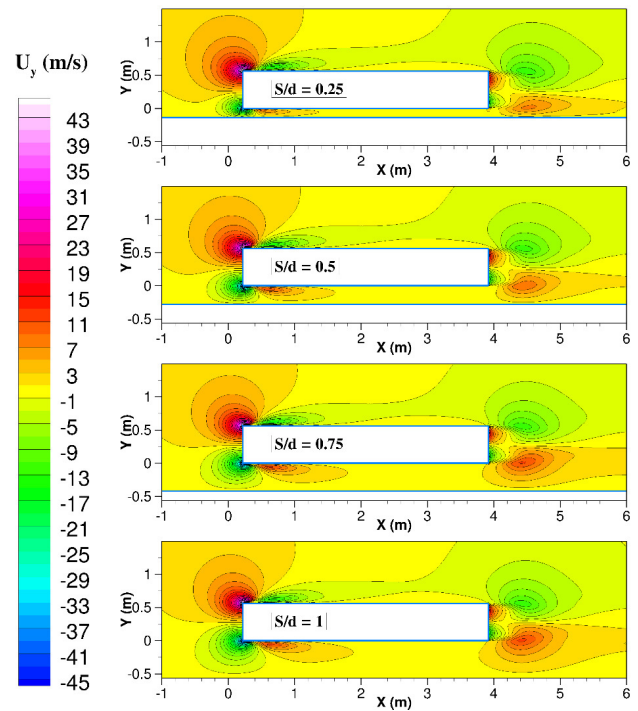

Fig. 13 Velocity field in the y-direction, U_y, for the four distances between the train and the lateral wall in the top view

Figs. 14 and 15 show the pressure distribution for the cases in two side and top views. As can be seen, distance changes have the most remarkable effects on the pressure distribution in the critical area between the train and the

lateral wall. The distance changes also change the pressure distribution structure in the crucial space between the train and the lateral wall and the other regions. Moreover, by decreasing the distance between the train and the wall,
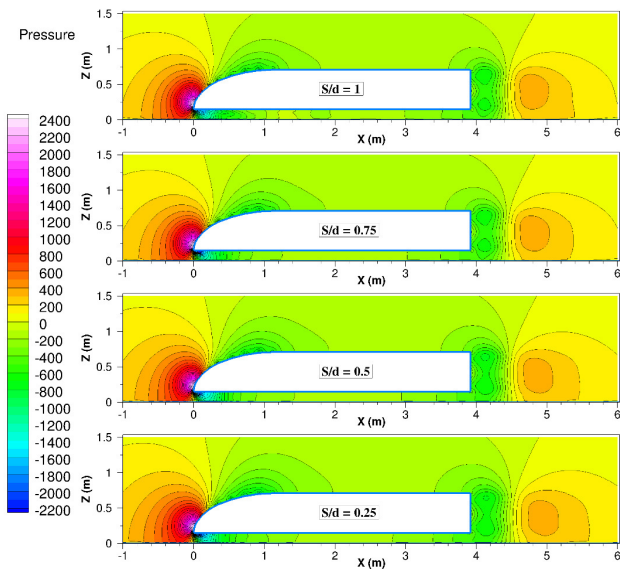
Fig. 14 Pressure field for the four distances between the train and the lateral wall in the side view
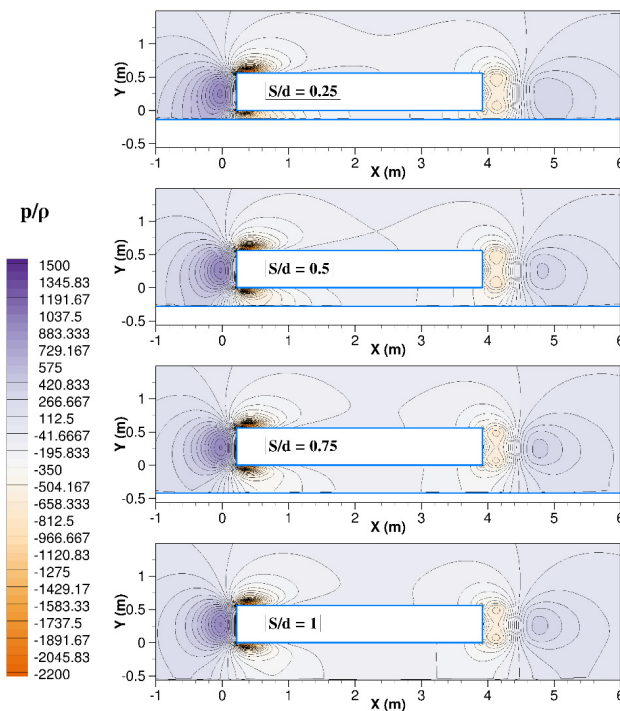

Fig. 15 Pressure field for the four distances between the train and the lateral wall in the top view

the pressure fields around the train become more comprehensive, more complicated, and more effective. Fig. 15 examines explicitly the ratio of pressure to the density of the turbulent air flow around the high-speed train, considering the lateral distances of the wall. The results indicate that at distances closer to the lateral wall, the pressure vortices at the beginning and end of the high-speed train are more connected, continuous, and asymmetric.

As this distance increases, the shape of these vortices is more symmetrical, and can be observed separately at the beginning and end of the train.

Another parameter defining turbulent flow characteristics is the turbulent kinetic energy, *k*. This parameter determines the level of flow turbulence. The changes of the turbulent kinetic energy for the four distances between the train and the lateral wall are depicted in Fig. 16. Fig. 16 shows that with increasing the distance between the train and the wall, the amount of turbulence in the air distance between the train and the ground and the back of the train increases. Also, with decreasing the distance between the train and the wall, the shape of turbulent kinetic energy becomes more elongated.

6 Conclusions
The natural features, such as mountain slopes, cliffs, and the human-made artificial walls, such as train station walls, windbreakers, and even residential and office buildings, can affect the movement structure of high-speed trains. So, since the effect of lateral walls along the train's movement was not sufficiently addressed, this research has addressed this relatively neglected sector. In this paper, applying the Reynolds-Averaged Navier-Stokes (RANS) equations and the *k-ω* (SST) turbulence approach, a turbulent air-flow around a simplified high-speed train is simulated. Also, a lateral wall parallel to the length of the train is considered, and for the four distances between them as and *S/k* = 0.25, 0.5, 0.75, and 1, influences of the distance changes on the aerodynamic and flow key parameters are
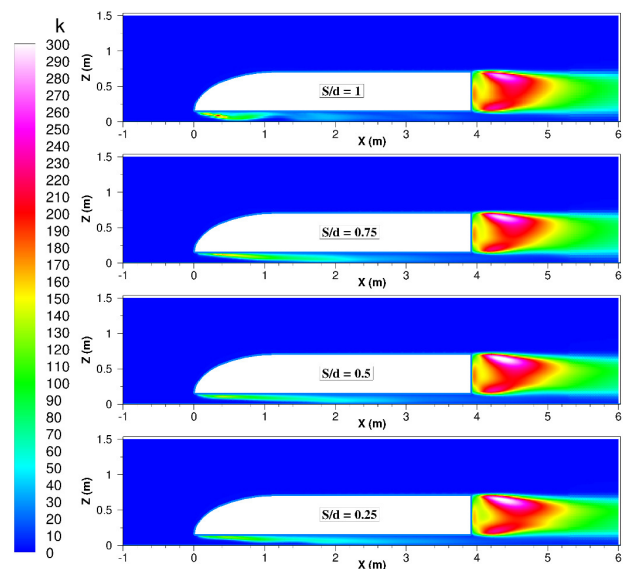

Fig. 16 Distribution of turbulent kinetic energy for the four distances between the lateral wall and the train

discussed. The first, the aerodynamic lift, drag, and side forces and their corresponding moments as pitching, yawing, and rolling for the distance changes are provided. The results illustrated that reducing the distance between them increases opposition forces and moments by 100 to 150 percent. In the following, the principal parameters of flow structure, i.e., streamline, velocity, and pressure distributions, and vortices structures, are shown for the four cases, individually. Parameter changes are affected by distance changes, clearly defining the vortex formation and more pressure when the train is closer to the lateral wall. Finally, the contour of the turbulent kinetic energy as an essential parameter in detecting the degree of turbulence for the four cases is presented. Based on this contour, the train's compartment is closer to the lateral wall, and the amount of turbulence on the back of the train is more than in other cases. Although, the turbulent rate in the air distance between the train and the ground is the highest amount in the distance between the train and the lateral wall. Overall, it seems that closer distance between the train and the wall has more destructive effects on the movement of the high-speed trains, although this is not a general and permanent issue. Anyway, a series of computational limitations plagued this research, the most important of which is the similarity ratio of natural obstacles with real examples. For future research, more realization of the high-speed train, and natural obstacles are considered. However, the obtained results of the present study can be helpful for designing structures along the rail and distancing it from natural features. Moreover, using the results of this research and similar research, it is possible to find solutions for better movement with the most negligible side effects caused by natural and artificial phenomena.

Nomenclature

Symbol	Quantity
A	Surface of the train (m^2)
C_D	Aerodynamic Drag coefficient
C_L	Aerodynamic Lift coefficient
C_S	Aerodynamic Side coefficient
C_{PT}	Pitching moment coefficient
C_{RL}	Rolling moment coefficient
C_Y	Yawing moment coefficient
d	Width and Height of the train (m)
F_D	Aerodynamic Drag force (kg m/s^2)
F_L	Aerodynamic Lift force (kg m/s^2)
F_S	Aerodynamic Side force (kg m/s^2)
k	Turbulent kinetic energy (m^2/s^2)
L	Length of the train (m)
P	Pressure (kg/m s^2)
R_{PT}	Pitching moment (kg m^2/s^2)
R_{RL}	Rolling moment (kg m^2/s^2)
R_Y	Yawing moment (kg m^2/s^2)
Re	Reynolds number
S	Distance between the lateral wall and the train (m)
t	Time (s)
u	Velocity (m/s)
U_∞	Free-stream velocity (m/s)
Greek symbol	Quantity
δ	Kronecker delta
ρ	Density (kg/m^3)
τ_{ij}	Effective stress tensor (kg/m s^2)
v	Kinematic viscosity (m^2/s)
v_t	Turbulent kinematic viscosity (m^2/s)
ω	Specific Dissipation Rate (1/s)
Index symbol	Quantity
i, j, k	Indices of the x, y, z-direction

References
[1] Rashidi, M. M., Hajipour, A., Li, T., Yang, Z., Li, Q. "A Review of Recent Studies on Simulations for Flow around High-Speed Trains", Journal of Applied and Computational Mechanics, 5(2), pp. 311–333, 2019.
https://doi.org/10.22055/jacm.2018.25495.1272

[2] Zhao, X., Sun, Z. A. "New Method for Numerical Simulation of Two Trains Passing by Each Other at the Same Speed", Journal of Hydrodynamics, 22(5), pp. 697–702, 2010.
https://doi.org/10.1016/S1001-6058(09)60105-0

[3] Baker, C. "The flow around high speed trains", Journal of Wind Engineering and Industrial Aerodynamics, 98(6–7), pp. 277–298, 2010.
https://doi.org/10.1016/j.jweia.2009.11.002

[4] Bell, J. R., Burton, Thompson, D. M., Herbst, A., Sheridan, J. "Wind tunnel analysis of the slipstream and wake of a high-speed train", Journal of Wind Engineering and Industrial Aerodynamics, 134, pp. 122–138, 2014.
https://doi.org/10.1016/j.jweia.2014.09.004

[5] Shuanbao, Y., Dilong, G., Zhenxu, S., Guowei, Y., Dawei, C. "Optimization design for aerodynamic elements of high speed trains", Computers & Fluids, 95, pp. 56–73, 2014.
https://doi.org/10.1016/j.compfluid.2014.02.018

[6] Niu, J., Liang, X., Zhou, D. "Experimental study on the effect of Reynolds number on aerodynamic performance of high-speed train with and without yaw angle", Journal of Wind Engineering and Industrial Aerodynamics, 157, pp. 36–46, 2016.
https://doi.org/10.1016/j.jweia.2016.08.007

[7] Munoz-Paniagua, J., García, J., Lehugeur, B. "Evaluation of RANS, SAS and IDDES models for the simulation of the flow around a high-speed train subjected to crosswind", Journal of Wind Engineering and Industrial Aerodynamics, 171, pp. 50–66, 2017.
https://doi.org/10.1016/j.jweia.2017.09.006

[8] Bell, J. R., Burton, D., Thompson, M. C., Herbst, A. H., Sheridan, J. "The effect of tail geometry on the slipstream and unsteady wake structure of high-speed trains", Experimental Thermal and Fluid Science, 83, pp. 215–230, 2017.
https://doi.org/10.1016/j.expthermflusci.2017.01.014

[9] Niu, J., Wang, Y., Zhang, L., Yuan, Y. "Numerical analysis of aerodynamic characteristics of high-speed train with different train nose lengths", International Journal of Heat and Mass Transfer, 127, pp. 188–199, 2018.
https://doi.org/10.1016/j.ijheatmasstransfer.2018.08.041

[10] Xia, C., Wang, H., Bao, D., Yang, Z. "Unsteady flow structures in the wake of a high-speed train", Experimental Thermal and Fluid Science, 98, pp. 381–396, 2018.
https://doi.org/10.1016/j.expthermflusci.2018.06.010

[11] Rocchi, D., Tomasini, G., Schito, P., Somaschini, C. "Wind effects induced by high speed train pass-by in open air", Journal of Wind Engineering and Industrial Aerodynamics, 173, pp. 279–288, 2018.
https://doi.org/10.1016/j.jweia.2017.10.020

[12] Mohebbi, M., Rezvani, M. A. "Multi objective optimization of aerodynamic design of high speed railway windbreaks using Lattice Boltzmann Method and wind tunnel test results", International Journal of Rail Transportation, 6(3), pp. 183–201, 2018.
https://doi.org/10.1080/23248378.2018.1463873

[13] Mohebbi, M., Rezvani, M. A. "Two-dimensional analysis of the influence of windbreaks on airflow over a high-speed train under crosswind using lattice Boltzmann method", Proceedings of the Institution of Mechanical Engineers, Part F: Journal of Rail and Rapid Transit, 232(3), pp. 863–872, 2018.
https://doi.org/10.1177/0954409717699502

[14] Mohebbi, M., Rezvani, M. A. "The Impact of Air Fences Geometry on Air Flow around an ICE3 High Speed Train on a Double Line Railway Track with Exposure to Crosswinds", Journal of Applied Fluid Mechanics, 11(3) pp. 743–754, 2018.
https://doi.org/10.29252/JAFM.11.03.27862

[15] Li, H., He, X., Wang, H., Kareem, A. "Aerodynamics of a scale model of a high-speed train on a streamlined deck in cross winds", Journal of Fluids and Structures, 91, 102717, 2019.
https://doi.org/10.1016/j.jfluidstructs.2019.102717

[16] Wang, S., Peng, Y., Wang, T., Chen, X., Hou, L., Zhang, H. "The origami inspired optimization design to improve the crashworthiness of a multi-cell thin-walled structure for high speed train", International Journal of Mechanical Sciences, 159, pp. 345–358, 2019.
https://doi.org/10.1016/j.ijmecsci.2019.06.017

[17] Hashmi, S. A., Hemida, H., Soper, D. "Wind tunnel testing on a train model subjected to crosswinds with different windbreak walls", Journal of Wind Engineering and Industrial Aerodynamics, 195, 104013, 2019.
https://doi.org/10.1016/j.jweia.2019.104013

[18] Zampieri, A., Rocchi, D., Schito, P., Somaschini, C. "Numerical-experimental analysis of the slipstream produced by a high speed train", Journal of Wind Engineering and Industrial Aerodynamics, 195, 104022, 2020.
https://doi.org/10.1016/j.jweia.2019.104022

[19] Dong, T., Minelli, G., Wanga, J., Liang, X., Krajnović, S. "The effect of ground clearance on the aerodynamics of a generic high-speed train", Journal of Fluids and Structures, 95, 102990, 2020.
https://doi.org/10.1016/j.jfluidstructs.2020.102990

[20] Xu, R., Wu, F., Zhong, M., Li, X., Ding, J. "Numerical investigation on the aerodynamics and dynamics of a high-speed train passing through a tornado-like vortex", Journal of Fluids and Structures, 96, 103042, 2020.
https://doi.org/10.1016/j.jfluidstructs.2020.103042

[21] Muñoz-Paniagua, J., García, J. "Aerodynamic drag optimization of a high-speed train", Journal of Wind Engineering and Industrial Aerodynamics, 204, 104215, 2020.
https://doi.org/10.1016/j.jweia.2020.104215

[22] Wang, D., Chen, C., Hu, J., He, Z. "The effect of Reynolds number on the unsteady wake of a high-speed train", Journal of Wind Engineering and Industrial Aerodynamics, 204, 104223, 2020.
https://doi.org/10.1016/j.jweia.2020.104223

[23] Xiao, C., Yang, M., Tan, C., Lu, Z. "Effects of platform sinking height on the unsteady aerodynamic performance of high-speed train pantograph", Journal of Wind Engineering and Industrial Aerodynamics, 204, 104284, 2020.
https://doi.org/10.1016/j.jweia.2020.104284

[24] Xiong, X. H., Yang, B., Wang, K. W., Liu, T. H., He, Z., Zhu, L. "Full-scale experiment of transient aerodynamic pressures acting on a bridge noise barrier induced by the passage of high-speed trains operating at 380–420 km/h", Journal of Wind Engineering and Industrial Aerodynamics, 204, 104298, 2020.
https://doi.org/10.1016/j.jweia.2020.104298

[25] Li, T., Hemida, H., Rashidi, M. M., Zhang, W. "The Impact of Numerical Divergence Schemes on the Flow Around Trains", Fluid Dynamics Research, 52(2), 025509, 2020.
https://doi.org/10.1088/1873-7005/ab8314

[26] Mohebbi, M., Safaee, A. M. "The Optimum Model Determination of Porous Barriers in High-Speed Tracks", Proceedings of the Institution of Mechanical Engineers, Part F: Journal of Rail and Rapid Transit, 236(1), pp. 15–25, 2022.
https://doi.org/10.1177/0954409721995323

[27] Mohebbi, M., Rezvani, M. A. "2D and 3D numerical and experimental analyses of the aerodynamic effects of air fences on a high-speed train", Wind and Structures, 32(6), pp. 539–550, 2021.
https://doi.org/10.12989/was.2021.32.6.539

[28] Mohebbi, M., Ma, Y., Mohebbi, R. "The Analysis of Utilizing Multiple Fences in High-Speed Tracks on the Aerodynamic Characteristics of a High-Speed Train Model", Iranian Journal of Science and Technology, Transactions of Mechanical Engineering, 2023.
https://doi.org/10.1007/s40997-023-00702-5

[29] Mohebbi, M., Ma, Y., Mohebbi, R. "The Influence of Inclined Barriers on Airflow Over a High Speed Train under Crosswind Condition", In: Hessami, A. G., Muttram, R. (eds.) New Research on Railway Engineering and Transportation, [e-book] IntechOpen, 2023.
https://doi.org/10.5772/intechopen.112751

[30] Hajipour, A., Lavasani, A. M., Yazdi, M. E. "Investigation of Wall Function Effects on Aerodynamic Characteristics of Turbulent Flow Around a Simplified High-Speed Train", International Journal of Heat and Technology, 39(1), pp. 309–318, 2021.
https://doi.org/10.18280/ijht.390134

[31] Hajipour, A., Lavasani, A. M., Yazdi, M. E. "A Computational Study on Aerodynamic Characteristics of a Simplified High-Speed Train: The Effects of Crosswinds and Surface Roughness", International Journal of Nonlinear and Applications, 12(Special Issue), pp. 519–540, 2021.
https://doi.org/10.22075/ijnaa.2021.23992.2647

[32] Hajipour, A., Lavasani, A. M., Yazdi, M. E. "LES Study on the Embankment Height Effect on the Aerodynamic Characteristics of a Generic High-Speed Train", Iranian Journal of Science and Technology, Transactions of Mechanical Engineering, 47(3), pp. 829–839, 2023.
https://doi.org/10.1007/s40997-022-00554-5

[33] OpenFOAM Foundation "OpenFOAM", [online] Available at: www.openfoam.org [Accessed: 14 April 2023]

[34] Tavangar, T., Tofighian, H., Tarokh, A. "Investigation of the Horizontal Motion of Particle-Laden Jets", Computation, 8(2), 23, 2020.
https://doi.org/10.3390/computation8020023

[35] Menter, F. R. "Two-Equation Eddy-Viscosity Turbulence Models for Engineering Applications", AIAA Journal, 32(8), pp. 1598–1605, 1994.
https://doi.org/10.2514/3.12149

[36] Sakuma, Y., Ido, A. "Wind Tunnel Experiments on Reducing Separated Flow Region Around Front Ends of Vehicles on Meter-Gauge Railway Lines", Quarterly Report of RTRI, 50(1), pp. 20–25, 2009.
https://doi.org/10.2219/rtriqr.50.20

[37] Ishak, I. A., Ali, M. S. M., Yakub, M. F. M., Salim, S. A. Z. S. "Effect of crosswinds on aerodynamic characteristics around a generic train model", International Journal of Rail Transportation, 7(1), pp. 23–54, 2019.
https://doi.org/10.1080/23248378.2018.1424573

[38] Hemida, H., Krajnović, S. "LES study of the influence of the nose shape and yaw angles on flow structures around trains", Journal of Wind Engineering and Industrial Aerodynamics, 98(1), pp. 34–46, 2010.
https://doi.org/10.1016/j.jweia.2009.08.012

[39] Zhuang, Y., Lu, X. "Numerical investigation on the aerodynamics of a simplified high-speed train under crosswinds", Theoretical and Applied Mechanics Letters, 5(5), pp. 181–186, 2015.
https://doi.org/10.1016/j.taml.2015.06.001

[40] Wang, Y., Thompson, D., Hu, Z. "Effect of wall proximity on the flow over a cube and the implications for the noise emitted", Physics of Fluids, 31(7), 077101, 2019.
https://doi.org/10.1063/1.5096072

[41] Nakaguchi, H. "Recent Japanese research on three-dimensional bluff-body flows relevant to road-vehicle aerodynamics", In: Sovran, G., Morel, T., Mason, W. T. (eds.) Aerodynamic Drag Mechanisms of Bluff Bodies and Road Vehicles, Springer, 1978, pp. 227–252. ISBN 978-1-4684-8436-6
https://doi.org/10.1007/978-1-4684-8434-2_9

[42] Raul, R., Bernard, P. S. "A numerical investigation of the turbulent flow field generated by a stationary cube", Journal of Fluids Engineering, 113(2), pp. 216–222, 1991.
https://doi.org/10.1115/1.2909483

[43] Anderson, H. "Investigation of the forces on bluff bodies near the ground", M.Sc. Thesis, Department of Aeronautics, Imperial College, 1977.

[44] Haider, A., Levenspiel, O. "Drag coefficient and terminal velocity of spherical and nonspherical particles", Powder Technology, 58(1), pp. 63–70, 1989.
https://doi.org/10.1016/0032-5910(89)80008-7

Appendix

The geometrical and flow characteristics of the research intended for validation are as follows. A surface-mounted cube with a height of $L = 0.6$ m against a turbulent flow with free-stream velocity as $U_\infty = 12.5$ m/s is assumed [40]. The corresponding Reynolds number $Re = U_\infty L/v = 50000$, where v is the kinematic viscosity [40]. Also, a computational domain with dimensions $26L \times 7L \times 13L$ is considered [40]. All the geometric details, computational domain, and considered boundary conditions can be seen in Fig. A1.

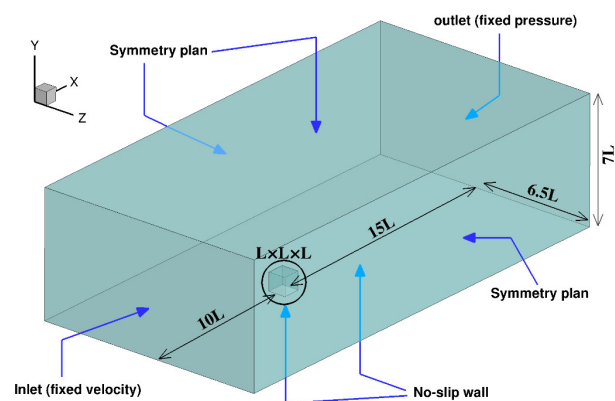**Fig. A1** Details of the geometry and computational domain for the validation [40]